MODELING OF SILICON CHARACTERISTICS IN THE SEMICONDUCTOR-METAL PHASE TRANSITION REGION

O.N. KOROLEVA[1,2], A.V. MAZHUKIN[1,2], V.I. MAZHUKIN[1,2]

[1]Keldysh Institute of Applied Mathematics
e-mail:vim@modhef.ru

[2]National Research Nuclear University MEPhI

Summary. In the temperature range of the semiconductor-metal phase transition by means of molecular dynamic modeling (MDM), the equilibrium properties of crystalline and molten silicon are determined. The pressure dependences of the specific heat of melting and the equilibrium melting temperature, the temperature dependences of the density, the linear size of the sample, the coefficient of linear expansion, enthalpy, and heat capacity are determined. The obtained dependences of the properties of silicon are approximated by polynomials of low degrees. The results of the comparison of the obtained characteristics of silicon with experimental data show an acceptable qualitative and quantitative agreement. Numerical and graphical information on the obtained properties and results of comparison with experimental data are presented.

1 INTRODUCTION

Crystalline silicon (c-Si) refers to one of the most common structural and technological materials. Thermodynamic, thermophysical, kinetic, and optical properties have been studied in a huge number of papers [1-5], and these studies do not stop at the present time [6-8].

Most of the properties of solids depend on the chemical composition (microstructure), atomic structure (arrangement of atoms) and body dimensions (1-d, 2-d or 3-d). The change in one or more of these parameters entails a change in the properties of the solid. An example is the synthesis of materials of the crystalline phase with new properties, by controlled manipulation of their microstructure at the atomic level [9].

An important direction in the use of crystalline silicon (c-Si) is the use as a constructional material in sources of renewable energy, in particular, solar [10]. Modules of solar panels are mostly assembled from crystalline silicon (c-Si) elements (plates). The solar energy in them is converted directly into the energy of the electric current as a result of the photovoltaic (PV) effect [11]. The production of solar silicon plates is associated with direct contact between the solid, liquid and gas phases under conditions close to the equilibrium state of melting-crystallization [12, 13].

Crystalline silicon is an indirect-gap semiconductor, and its electrical properties largely depend on the presence of defects and impurities (which are captured by charge carriers). The desired level of impurity concentration, on which the microstructural changes in silicon depend [14], is usually achieved by choosing the treatment temperature, which influences the diffusion of impurity atoms. A high diffusion coefficient in the melt facilitates creation of large bulk Si-substrates with uniform distribution of the dopant.

Examples of technological applications of crystalline silicon in nano- and microelectronic devices, the properties of which are determined by procedures for changing the chemical

2010 Mathematics Subject Classification: 82C26, 68U20, 74A15.
Key words and Phrases: Molecular Dynamic Modeling, Phase Transition, Silicon, Equilibrium Thermophysical Properties.

composition and atomic structure on the nanometer scale by means of ion implantation [15-17], thermal [7, 18] and laser processing [19, 20].

Even under slow thermal action under conditions close to thermodynamic equilibrium in crystalline silicon, a number of structural transformations are observed, accompanied by a successive transition (at temperatures far from the melting temperature T <Tm) from covalent to covalent-metal and to close-packed metallic structures at T~ Tm. Thus, at the heating rate ≈ 5 deg/min [18, 21] of dislocation-free silicon, the following sequence of structural transformations is observed: from fcc at 523K <T <593K to orthorhombic at 593K <T <803K and II hexagonal at 803K <T <943K. Near the melting temperature Tm, bct structures arise at 1473 K <T <1673 K and bcc at T> 1673. Polymorphic transformations in silicon, which occur when a substance passes from one crystalline state to another, affect not only the lattice parameter, but also its thermophysical, optical, mechanical, electrical, and kinetic properties [18, 21]. In the vicinity of the phase transition point, all the properties of crystalline silicon undergo qualitative changes and differ significantly from those of metals.

Because of this, it is important to use the theoretical approach to obtain the properties of the material under study, the main tool of which is mathematical modeling based on atomistic models, which over the past two decades has become a powerful tool for fundamental research of properties [22 -24] and processes [25 -27] in materials.

The purpose of this article is to determine, using molecular dynamic modeling, the equilibrium properties of crystalline and molten silicon in the temperature range associated with melting and crystallization of microstructures.

2 MODELING OF THE PROPERTIES OF THE PHONON SUBSYSTEM OF SILICON

The determination of the thermophysical properties of the phonon subsystem of silicon in this paper is based on the atomistic approach.

Atomistic models are a system of differential equations describing the aggregate of interacting particles (atoms, ions, molecules). When using atomistic models to study various properties of substances, the important role is played by the choice of interaction potentials between particles, since the reliability of the results obtained directly depends on it. The construction of the interatomic interaction potential for silicon has a number of peculiarities. The interatomic interaction in silicon is more complex than in metals.

Therefore, in order to determine the applicability of the selected interaction potentials under certain specific conditions, the use of atomistic models requires careful test calculations. This problem is especially acute in materials with covalent bonds, to which silicon belongs.

MD simulation was used to determine the silicon macro parameters - the pressure dependences of the melting temperature and the heat of the melting transition and the temperature dependences of the heat of evaporation, heat capacity, and linear expansion. These parameters can be determined with an accuracy of ≈ 1÷3%. In the rest, the accuracy of the calculation of properties is determined by the molecular interaction potential. On the basis of the analysis of the interaction potentials in [23], the potentials of Stillinger-Weber (SW) and KIHS are used in this study [28-30].

2.1 Mathematical model

The molecular dynamics (MD) method is based on the model representation of a polyatomic molecular system in which N particles are represented by material points, each of which has a mass, radius vector and velocity, respectively, $m_i, \vec{r}_i, \vec{\upsilon}_i$ where $i = 1 \ldots N$. Interaction between particles is carried out by means of forces $\vec{F}_i = -\dfrac{\partial U(\vec{r}_1 \ldots \vec{r}_N)}{\partial \vec{r}_i}$ where $U(\vec{r}_1 \ldots \vec{r}_N)$ is potential energy of interaction of a system of N particles; interaction with external fields occurs through force. The motion of an ensemble of particles in the classical case is described by Newton's equations.

As a result, the mathematical formulation of the problem consists of a system of ordinary differential equations, their difference analogue (difference scheme), interatomic interaction potential, and specifically defined initial and boundary conditions. The evolution of an ensemble of particles is described by a system of 2N ordinary differential equations of motion:

$$\begin{cases} m_i \dfrac{d\vec{\upsilon}_i}{dt} = \vec{F}_i + \vec{F}_i^{ext} \\ \dfrac{d\vec{r}_i}{dt} = \vec{\upsilon}_i \qquad i = 1 \ldots N \end{cases} \tag{1}$$

Knowledge of the coordinates and velocities at the initial time t=0 of all N particles is required to integrate the system of equations (1).

2.2 Initial conditions

At the initial time the simulated medium is a crystal, polycrystal or liquid. To more accurately set the initial values of macroscopic parameters and also to ensure a stable state of the system, after the coordinates and velocities are set, equilibration of the modeled ensemble is carried out.

The combined use of a thermostat and a barostat, which returns energy to the chaotic component of the particle motion to keep the target temperature and pressure, allows the system to be brought to state of thermodynamic equilibrium quickly enough. After the system is brought to rest, several changes in the lattice constant, taking into account the influence of the boundaries of the object, will be obtained automatically. A procedure for the formation of initial conditions is given in [32].

2.3 Boundary conditions

In the case of using the viewing area of the infinite one, two or three spatial directions X Y Z, the simulation of the processes is performed in the final computational domain with dimensions $L_x \times L_y \times L_z$ along the X Y Z axes, respectively. To simulate the interaction in the part that does not enter into the calculation area, the X, Y or Z axes use periodic boundary conditions with L_x, L_y, L_z periods respectively.

Periodic boundary conditions, for example, in X it means that particles with a coordinate x within the range $0 \le x < L_x$, accurately reproduce the particles $kL_x \le x < (k+1)L_x$ for any

integers $k \neq 0$. That is, the particle leaving the calculation domain through the upper boundary $x = L_x$ is replaced by a particle with the same velocity value, but entered the calculation domain through the lower boundary $x = 0$. If we mark the quantities related to a new particle with a stroke, then

$$\begin{cases} \vec{\upsilon}' = \vec{\upsilon} \\ x' = (x - L_x) \quad \in \quad [0, L_x), \;\; L_x \le x < 2L_x \\ y' = y \\ z' = z \end{cases} \tag{2}$$

Similarly, for a particle leaving the calculation domain through the lower boundary:

$$\begin{cases} \vec{\upsilon}' = \vec{\upsilon} \\ x' = (x + L_x) \quad \in \quad [0, L_x), \;\; -L_x \le x < 0 \\ y' = y \\ z' = z \end{cases} \tag{3}$$

The second important aspect of periodic boundary conditions is the force and potential energy of interaction for particles from the boundary regions: $0 \le x < r_{cr}$ and $(L_x - r_{cr}) \le x < L_x$, where r_{cr} is the radius of potential cutoff (it is assumed that the interaction forces at $r > r_{cr}$ distances can be neglected).

The interaction of a particle i whose coordinate x_i is in the interval $(L_x - r_{cr}) \le x_i < L_x$ with particles outside the computational domain $L_x \le x'_j < (L_x + r_{cr})$ is modeled using $0 \le x_j < r_{cr}$ particles from the computational domain whose radius vectors are corrected as follows in calculating the interaction force $\vec{F}_{ij} = \vec{F}_{(\ldots \vec{r}'_j \ldots)}(\vec{r}_i)$:

$$\vec{r}'_j = \vec{r}_j + \vec{e}_x L_x ,$$

where $\vec{e}_x$ is single unit axis of the X axis.

Obviously, all of the foregoing applies equally to periodic boundary conditions along the coordinate axes Y and Z.

2.4 Potentials of interaction of particles

A comparison of a number of semi-empirical potentials in [23] showed that the Stillinger-Weber [28, 29] and KIHS potentials are the most suitable for the modeling of solid silicon over a wide range of pressures and temperatures [30, 31]. Therefore, in this paper, these potentials were used in the MD modeling of the properties of the phonon gas of silicon.

2.5 Computational algorithm

Molecular dynamics modeling of the mechanical and thermophysical properties of single-crystal silicon over a wide range of temperatures and pressures was carried out using the

widely used LAMMPS (Large-scale Atomic / Molecular Massively Parallel Simulator) application package [33]. It supports many pair and many-particle short-range potentials, it is possible to write atomic configurations in a text file, and also thermostats and barostats are built in. The computational algorithm is based on the Verlet finite-difference scheme [34].

The velocity and pressure corrections for the ensemble of particles were carried out with the help of Berendsen thermostat and the barostat [35].

A more detailed description of the mathematical formulation of the problem and its numerical realization can be found in [32].

3 RESULTS OF MODELING

The results of MDM for convenience of further use are approximated by power polynomials of degree m

$$P_{\mathrm{m}}(\mathrm{x}) = \sum_{k=0}^{m} a_k x^k \tag{4}$$

where a_k are polynomial coefficients.

The approximation error was calculated by the criterion of least squares

$$\Delta\left(P_m\left(t_j\right),\mathrm{y_j}\right) = \sqrt{\frac{1}{n+1}\sum_{j=0}^{n}\left(P_m\left(t_j\right)-y_j\right)^2} \to \min \tag{5}$$

where y_i are the MDM results for the arguments t_j (j = 0, ..., n).

3.1 Equilibrium temperature and specific heat of melting

To study the properties of matter in the region of the melting-crystallization phase transition, it is very important to know the relation of the melting point (Tm) to the pressure (P), since one and the same substance, depending on the value of the parameters (P, Tm), can be in any of the three groups - metal, semiconductor, dielectric, regardless of the predominance of the type of chemical bond. The ranges of pressure and temperature values, within which this substance remains in the same state, are wide enough. It is known [18, 36] that at high pressure (~ 12 GPa for silicon), a transition from a purely covalent diamond structure (K = 4) to a covalent metal bct structure of the β-Sn type was noticed, and then (~ 16 GPa) to typically bcc metal structure (K = 6). At compression in the temperature range 400-700°C, hexagonal silicon [37] is documented, which, apparently, is a metastable phase. At present, the phase diagrams of most materials remain relatively unknown outside the range of the normal conditions due to technical problems associated with conducting accurate phase behavior studies at extreme temperatures and/or pressures. MD modeling allows to determine the baric dependence of the melting temperature by means of a series of experiments. The simulation was carried out with SW and KIHS interaction potentials.

For numerical experiments, a calculated region in the form of a parallelepiped was filled with 16000 particles interacting via SW or KIHS potentials. At the initial stage, all particles are located at the sites of the fcc crystal lattice. The dimensions of the region are 20×10×10 elementary lattice cells. In all three spatial directions, the periodic boundary conditions (2), (3) are imposed on the boundaries of the computational domain; i.e. simulated object is an infinite single crystal of silicon. Before the series of molecular dynamics calculations, the

procedure for establishing the initial thermodynamic equilibrium in the ensemble of sample particles is carried out.

The procedure for establishing thermodynamic equilibrium in the system includes the following actions:

- Initial particle velocities are set at a temperature of 600 K,
- A thermodynamic equilibrium is established in the system, for which an equilibration calculation is started with the barostat turned on (with a target pressure of 0 bar) for a time of 20 ps with an integration step of 1 fs. The crystal temperature in 5-10 ps decreases to about 300 K.
- The thermostat is switched on, by which the entire calculation domain is first heated to 900 K (at zero pressure), and then half of the crystal is melted in the calculation domain, and in this half the temperature initially rises smoothly to 1600 K, and then again falls to 900 K.

The prepared sample contains the liquid and crystalline phases in contact at a temperature of 900 K and zero pressure.

The equilibrium melting temperature. As a result of computational experiments performed with potentials SW and KIHS, the baric dependences of the equilibrium melting temperature shown in Fig. 1 (indicated by hollow circles) were obtained. The baric dependence of the equilibrium melting temperature $T_m(P)$ is the equilibrium boundary between two phases of silicon, solid and liquid.

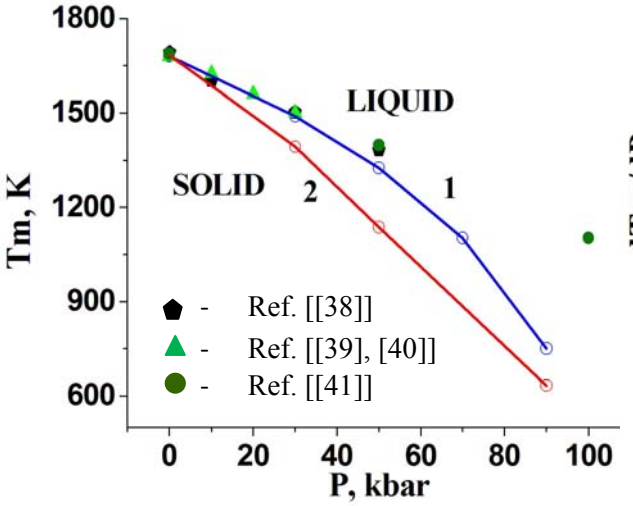

Figure 1. The baric dependences of the equilibrium melting temperature, calculated with the potentials (hollow circles) and their approximations (solid lines) (1) - SW, (2) - KIHS. Markers indicate reference and experimental data.

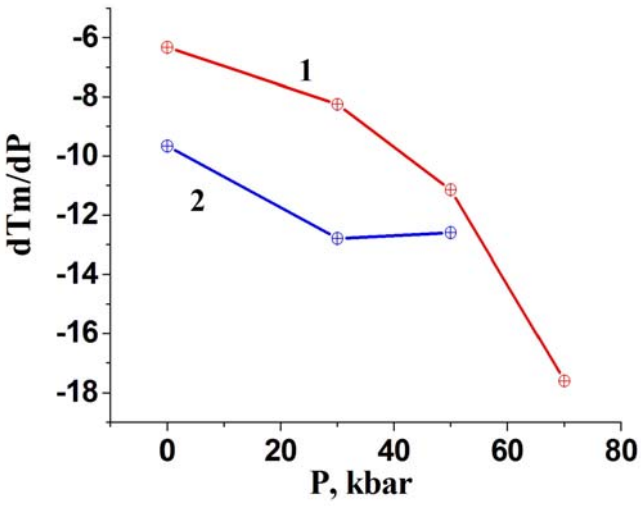

Figure 2. The baric melting point coefficients calculated with the potentials (1) - SW, (2) - KIHS.

The color markers in Fig. 1 denote reference [38] and experimental data [39-41]. The MDM results of the equilibrium melting temperature $T_m(P)$ were approximated by power polynomials (4).

For the potential SW: $$T_{m,SW}(P) = a_0 + a_1 P + a_2 P^2 + a_3 P^3 + a_4 P^4$$

For the potential KIHS: $T_{m,KIHS}(P) = a_0 + a_1 P + a_2 P^2 + a_3 P^3$

The values of the coefficients a_k and the least squares fit errors (5) are presented in Table 1.

k	SW a_k	KIHS a_k
0	1679.99999	1683.000
1	-4.759226	-6.686666
2	-0.077470	-0.121333
3	0.00116369	0.000733
4	-0.000011	
$\Delta(P_m(t_j),y_j)$ %	8.036×10^{-7}	1.295×10^{-8}

Table 1. Values of the coefficients of the function approximating Tm (P) from the results of MDM and the magnitude of the approximation error.

The simulation results with SW potential give better agreement with the experimental and reference data than the results of MDM with KIHS. However, with increasing pressure, the degree of coincidence with the reference data changes from almost complete in the low-pressure region (up to 40 kbar), to a discrepancy of ≈ 4.5% at 50 kbar and ≈ 47% at 90 kbar.

Silicon refers to substances in which the melting point decreases with increasing pressure. From the values of $T_m(P)$ obtained with different potentials, the baric melting point coefficients were calculated as the ratio of the differences

$$dT_m/dP \approx \Delta T_m/\Delta P .$$

The values of the pressure coefficients obtained for both potentials (Fig. 2) are given in Table 2. The table also shows the values of the coefficients obtained from the experimental values. As can be seen, the coefficients calculated from the MDM data are negative and decrease with increasing pressure;

Computational experiment data. SW potential.		Computational experiment data. KIHS potential.		Data from [[38]]		Data from [[39]]	
P (kbar)	$\Delta T_m/\Delta P$	P(kbar)	$\Delta T_m/\Delta P$	P(kbar)	$\Delta T_m/\Delta P$	P(kbar)	$\Delta T_m/\Delta P$
0	-6.333	0	-9.667	0.1	-8.99	0	-5.5
30	-8.25	30	-12.8	10	-5	10	-6.5
50	-11.15	50	-12.6	30	-6	20	-6
70	-17.6	90		50		30	
90							

Table 2. Values of the pressure coefficients of the equilibrium melting point.

The data shown in Fig. 1, 2 and in Table 2 indicate that within 50 kbar the experimentally determined values of the melting points of silicon are close to those obtained in the course of computational experiments.

Latent heat of melting. Latent heat of Si melting was calculated from the MD simulation data as the difference between the enthalpy of solid and liquid parts at the same temperature

and pressure. From the reference data, the values of the heat are known only at zero pressure of 49.9 KJ/mol [38] and 45.3 [42]. Despite the noticeable difference at zero pressure calculated data from reference ~ (30-50)%, both potentials show a qualitatively correct pressure dependence $L_m(P)$, Fig. 3, when the higher melting point Tm corresponds to higher values of the specific heat of melting $L_m(P)$.

The MDM results with SW and KIHS potentials were approximated by power polynomials (4)

$$L_m(P) = \left(a_0 + a_1 P + a_2 P^2 + a_3 P^3\right)_{SW,KIHS}$$

and are shown in Fig. 3.

The values of the coefficients a_k and the approximation errors by the criterion of least squares (5) are presented in Table 3.

k	SW a_k	KIHS a_k
0	32000.00	35000.00
1	-1066.66666	-1497.61905
2	-249.99999	-235.71428
3	16.66666	19.047619
$\Delta(P_m(t_j),y_j)$ %	3.821×10^{-7}	2.981×10^{-7}

Table 3. Values of the coefficients of the function approximating $L_m(P)$ from the results of MDM and the magnitude of the approximation error.

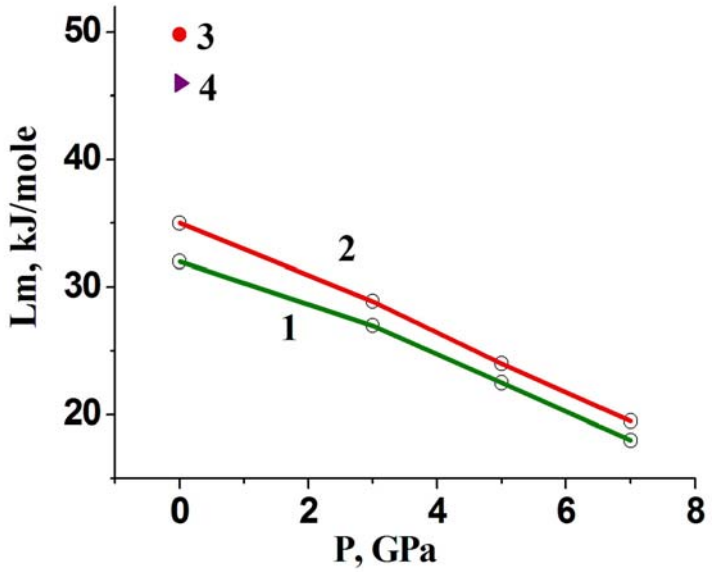

Figure 3. Heat of melting of Si by the results of MDM, for the interaction potentials (1) SW and (2) KIHS. Color markers refer to reference data (3) - [38]; (4) to [42].

3.2 Density, coefficient of linear expansion and heat capacity.

To understand the nature of the processes that occur during the heating of silicon and the transition from solid to liquid state, studies of density and linear expansion are of particular interest. From the series of molecular dynamics calculations within the framework of one computational experiment, the temperature dependences of the coefficient of linear expansion of $\alpha(T)$, density $\rho(T)$ and specific heat capacity $C_p(T)$ of silicon were determined. We used a cubic computational domain containing a fcc crystal of 8,000 particles. The heating range is 300÷4000K. The simulation was carried out with SW and KIHS interaction potentials. Temperature dependences were recorded: the density $\rho(T)$, enthalpy $H(T)$, and the linear size $L(T)$. The experiment was carried out at a constant zero pressure $P=0$.

Density. A lot of works have been devoted to investigations of the density of silicon melt by both domestic and foreign authors, nevertheless, interest in this problem is not weakening, as evidenced by numerous publications [43-46].

In this paper, a temperature dependence of the silicon density in the temperature range 300K≤T≤4000K is obtained from MDM. The results of the simulation after the necessary statistical processing are shown in Fig. 4. The density of the silicon melt at the equilibrium melting point (Tm = 1685 ° K) for both potentials is greater than the density of the crystals at the same temperature, i.e. silicon melts with compacting, just as it was observed in experiments [18, 21, 42-49].

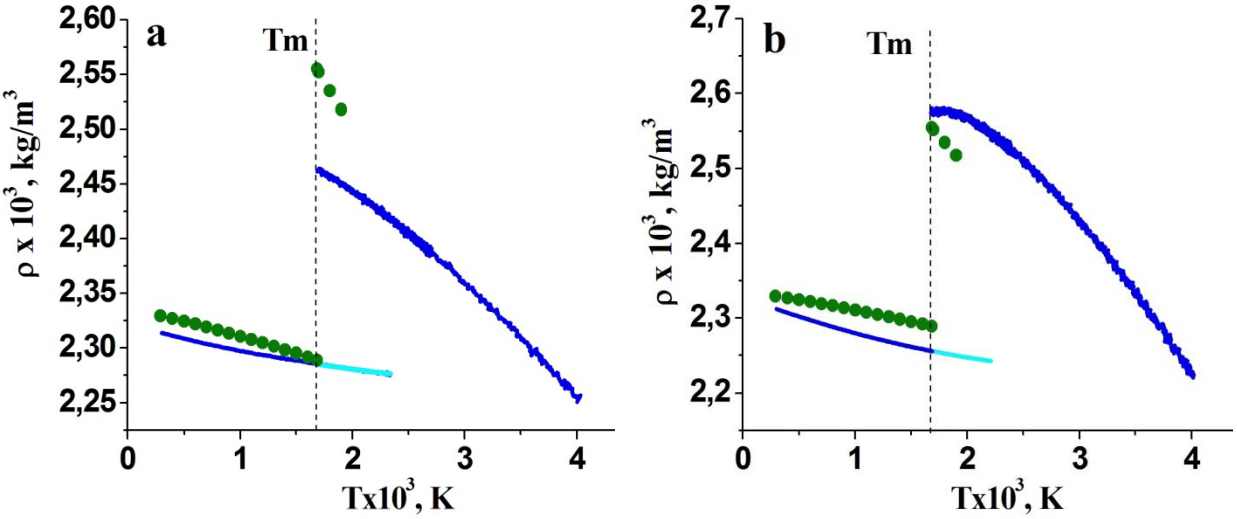

Figure 4. Temperature dependences of the density of silicon by the results of MDM (dark blue lines) and overheating of the solid phase (blue lines) for the potentials (a) - SW, (b) – KIHS, green markers are experimental data [46] for the potentials

In Fig. 4, a decrease in the density when the solid phase is superheated ($T > T_m$) is clearly noticeable. At equilibrium melting temperature T_m, a density jump occurs. The magnitude of the jump differs in calculations with different potentials. For the SW potential, the difference in the density values in the solid and liquid phases at the temperature $T=T_m$ is 7.75%, and for the KIHS potential - 14.15%. The estimate of the density jump in accordance with the experimental data differs from ~ 9 [49] to 11.62% [46]. Comparison of the simulation results

with the experimental data shows that the results of modeling with the KIHS potential for molten silicon are closer to the experimental data (Fig. 4b). For the density of the solid phase, the best fit with experiment is shown by the simulation results with SW potential (Fig. 4 a). The results of MDM show that the melting process leads to a significant increase in the density of silicon. The results obtained in the calculations are more convenient to use in the form of an analytical dependence of the form (4). For a solid phase, the dependence for both potentials is:

$$\rho_{sol}(T) = \left(a_0 + a_1(T - T_0)\right)_{SW,KIHS}$$

For the liquid phase $$\rho_{liq}(T) = \left(a_0 + a_1(T - T_m) + a_2(T - T_m)^2 + a_3(T - T_m)^3\right)_{SW}$$

$$\rho_{liq}(T) = \left(a_0 + a_1(T - T_m) + a_2(T - T_m)^2 + a_3(T - T_m)^3 + a_4(T - T_m)^4\right)_{KIHS}$$

The values of the coefficients a_k and the least squares approximation errors (5) are presented in Table 4.

k	SW, a_k		KIHS, a_k	
	Solid, T_0 = 300K	**Liqid, T_m = *1685K***	**Solid, T_0 = 300K**	**Liqid, T_m = *1685K***
0	2.313159	2.46305924	2.3065089	2.5743114
1	-1.80261528×10^{-5}	-8.19973366×10^{-5}	-3.5766095×10^{-5}	4.2675839×10^{-5}
2		7.364843×10^{-9}		-2.54372617×10^{-7}
3		$-3.990398848\times10^{-12}$		$1.813214833\times10^{-10}$
4				$-7.182882532\times10^{-14}$
Δ($P_m(T_i)$,y_i) %	0.106	0.885	0.233	0.291

Table 4. Values of the coefficients of functions approximating the density of silicon by the results of MDM and the magnitude of the approximation error.

Coefficient of linear expansion. The change in the linear size of the sample *L(T)* is closely related to the change in density. According to the results of MDM at the melting point T_m, the linear size of the molten sample was less than the linear size of the solid sample $L_{liq}(T) < L_{sol}(T)$ (Fig. 5), while the ratio of the melt density to the solid phase of silicon $\rho_{liq}(T) > \rho_{sol}(T)$ turned out to be inverse (Figure 4), which is an indicator of the silicon condensation during melting and corresponds to the experimental data [18, 21, 42-48]. In Fig. 5, it is seen that $L_{sol}(T)$ continues to increase when the solid phase overheats. The resulting overheats were $\Delta T_{SW} = 715$K and $\Delta T_{KIHS} = 565$K. The jump in the linear size at $T=T_m$ are 2.5% for the SW potential, and 4.5% for the KIHS potential.

According to the simulation results, the linear size of the molten sample turns out to be less than that of the solid sample, which shows as well as an increase in density during the phase transition, the compaction of silicon during melting, which corresponds to the experimental data [18, 21, 42-44]. The temperature dependences of the linear size of the silicon sample *L(T)* from the results of MDM are shown in Fig. 5. In Figure 5 it can be seen that the linear size of the sample continues to increase when the solid phase overheats during melting ($T \approx 2400 > Tm$), and at overcooling during crystallization ($T \approx 1420 < T_m$), the linear size of the sample continues to decrease. The jumps in the linear size at $T=T_m$ are 2.5% for the SW potential, and 4.5% for the KIHS potential.

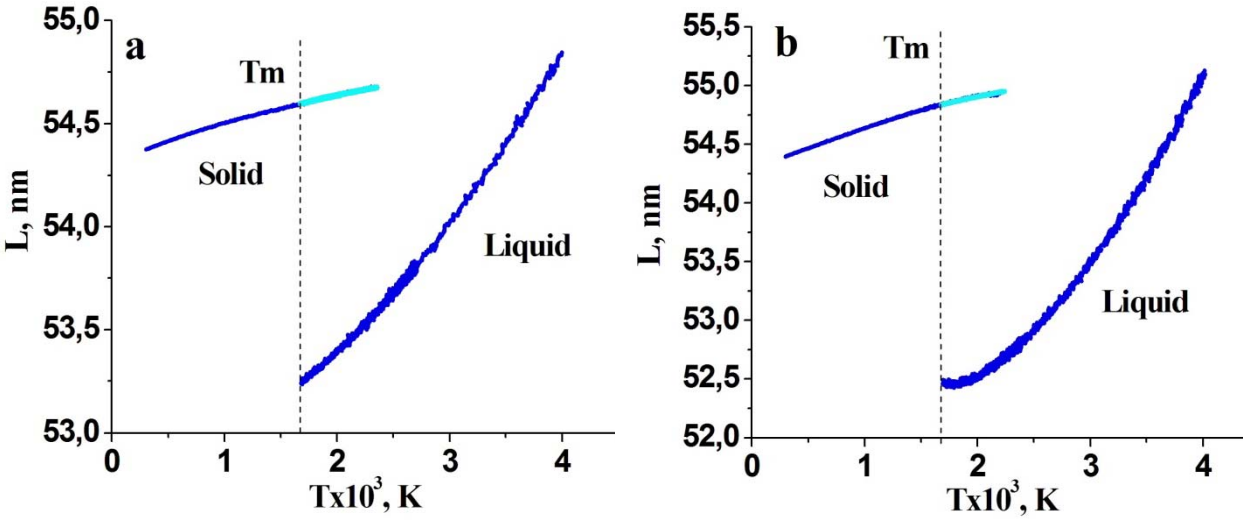

Figure 5. Temperature dependences of the linear size of the silicon sample from the results of MDM (dark blue lines) and overheating of the solid phase (blue lines) for the potentials a - SW, b – KIHS.

The temperature dependences of *L(T)* obtained from computational experiments were approximated by polynomials $\tilde{L}(T)$ of the form (4) for the solid and liquid phases. The coefficients of linear expansion at a pressure *P* were calculated according to the relationship

$$\alpha(\mathrm{T}) = \frac{1}{\tilde{L}(T)}\left(\frac{\partial \tilde{L}(T)}{\partial T}\right)_P \qquad (6)$$

The temperature dependences were approximated by power polynomials (4). For the solid and liquid phases, a second-degree dependences was obtained for both potentials:

$$\alpha_{sol,liq}(T) = \left(a_0 + a_1(T - T_0) + a_2(T - T_0)^2\right)_{SW,KIHS}$$

The values of the coefficients a_k and the least squares fit errors (5) are presented in Table 5.

	SW, a_k		KIHS, a_k	
k	**Solid, T_0 = 300K**	**Liqid, T_m = *1685K***	**Solid, T_0 = 300K**	**Liqid, T_m = *1685K***
0	2.258853×10^{-4}	4.396243×10^{-4}	1.599456005×10^{-6}	5.829544175×10^{-6}
1	-1.3080981×10^{-7}	2.36116978×10^{-7}	$1.262783137\times10^{-10}$	-1×10^{-9}
2	4.10776503×10^{-11}	$-1.30695502\times10^{-11}$	$-3.487407698\times10^{-13}$	$1.93112229992\times10^{-12}$
Δ($P_m(T_j)$,y_j) %	0.138	1.157	1.129×10^{-3}	0.644

Table 5. Values of the coefficients of the functions approximating the coefficient of linear expansion of silicon by the results of MDM and the magnitude of the approximation error.

A graphical representation of the results of modeling of the coefficient of linear expansion of silicon for various interaction potentials in the temperature range 300-4000 K and experimental data [18, 47, 48] is presented at Fig. 6.

The obtained results show qualitative agreement with the experimental data. However, the SW potential provides a better fit to the experimental data in the solid phase, and the KIHS potential -in the liquid phase.

With increasing temperature, the coefficient of linear expansion of silicon increases in the solid and liquid phases, which corresponds to the experimental data. According to the simulation results, the most intensive growth of the coefficient of linear expansion is observed at a temperature $T > T_m$, which indicates a decrease in the strength of interatomic bonds in the liquid phase of silicon.

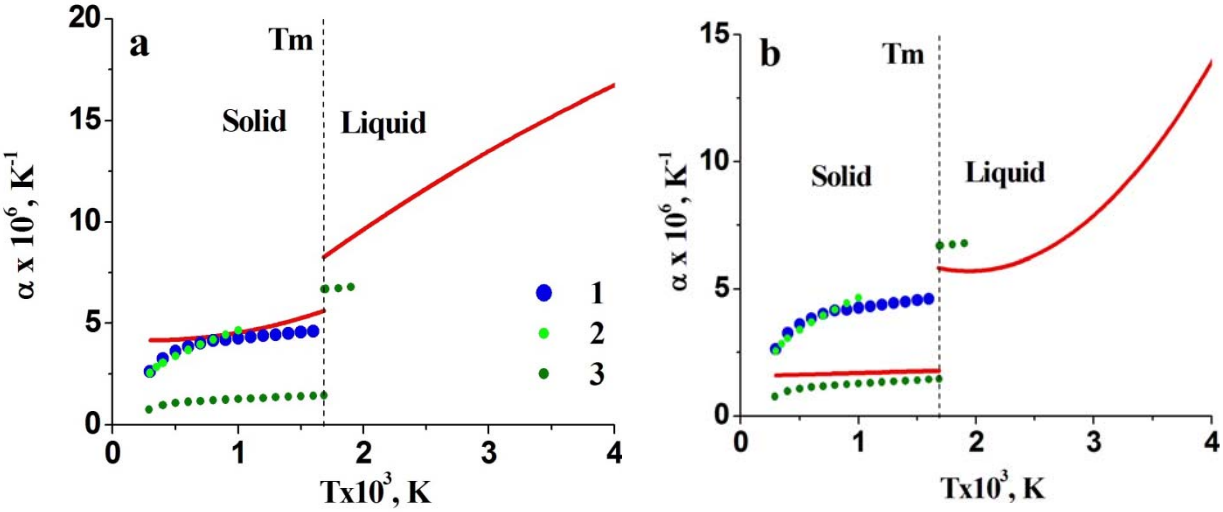

Figure 6. Temperature dependences of the coefficient of linear expansion of silicon. Red lines are graphs of functions that approximate the results of MD modeling for the potentials a-SW, b-KIHS. Experimental data: markers 1 - [48], 2 - [47], 3 - [46].

Specific heat. As is known, the specific heat is a measure of the energy absorption by matter when it is heated. The total specific heat $C(T, N)$ is determined by the specific heat of the lattice $C_{lat}(T)$ and the specific heat of free carriers $C_e(T,N)$ (electrons and holes), since the transfer of thermal energy in a solid is carried out by free charge carriers and phonons

$$C(T,N) = C_{lat}(T) + C_e(T,N) \qquad (7)$$

where N is the concentration of charge carriers.

In contrast to the specific heat of metals, for which the electronic component plays the dominant role at low temperatures and the main contribution is made by the lattice specific heat with increasing temperature. In silicon, the contribution of the electronic component to the total specific heat is small, but increases with increasing temperature and at the melting temperature T_m=1685 K is 1.4%, and at T=2000K - 1.72% [51]. Thus, the specific heat of the lattice makes the main contribution to the total specific heat, and the determination of its temperature dependence is an important problem, especially in the region of phase transition and in the range of higher temperatures.

The temperature dependence of the specific heat of the lattice at constant pressure was determined from the values of enthalpy $H(T)$ obtained in the course of the above-considered computational MDM experiment. The values of $H(T)$ were approximated for SW and KIHS

potentials separately for the liquid and solid phases by polynomials (4) of degree m=3÷5 (Fig. 7). The temperature dependence of the specific heat $C_{lat}(T)$ was determined by differentiation:

$$C_{lat}(T) = \left(\frac{\partial \tilde{H}(T)}{\partial T} \right)_P \qquad (8)$$

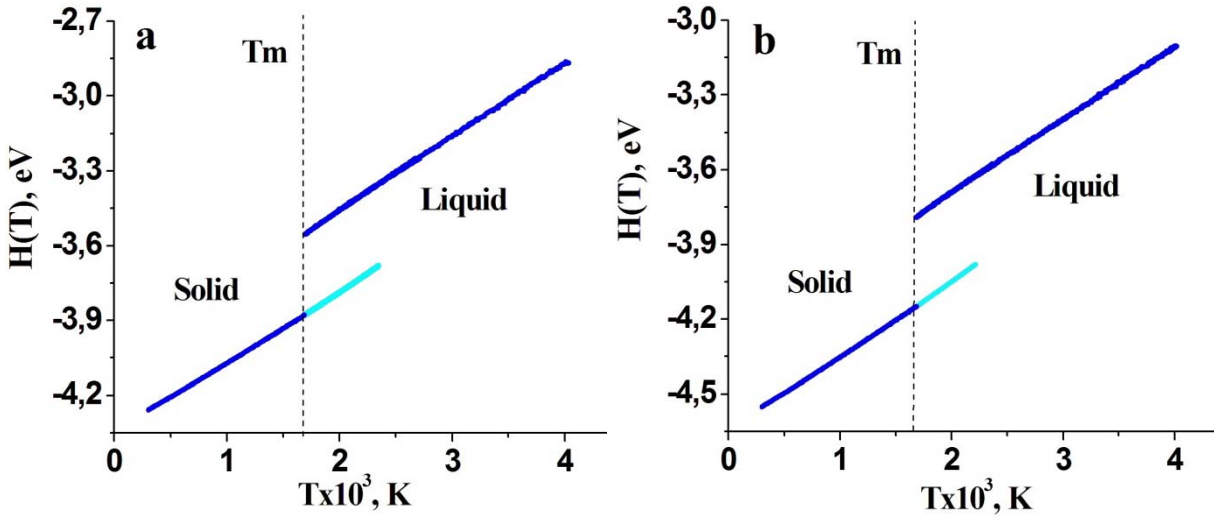

Figure 7. Temperature dependences of silicon enthalpy according to the results of MDM (dark blue lines) and overheating of the solid phase (blue lines) for the potentials a - SW, b - KIHS.

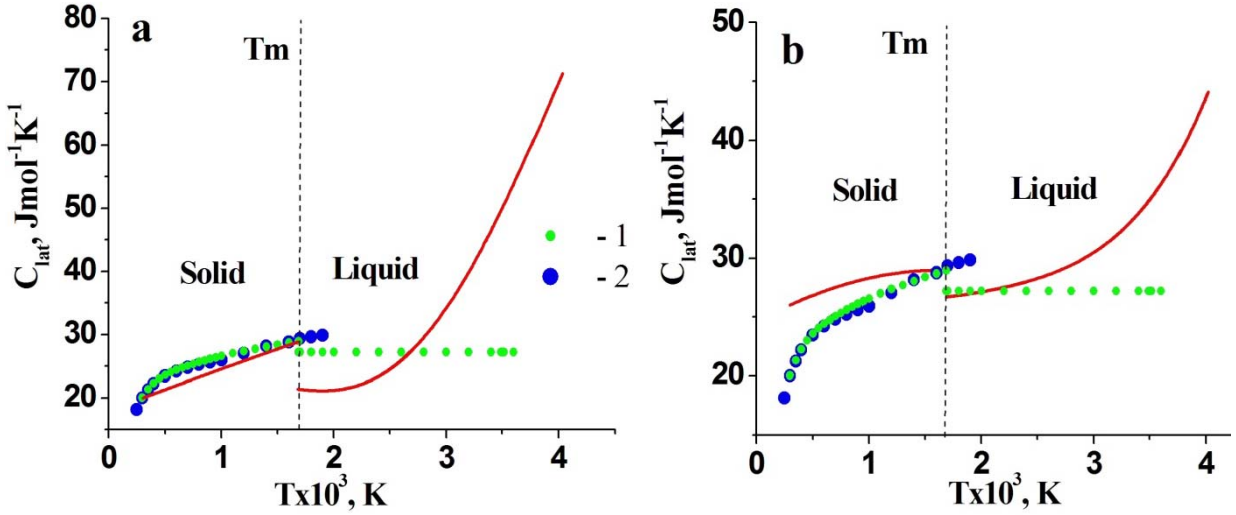

Figure 8. Temperature dependences of the specific heat of silicon. Red lines are approximating functions for the potentials a - SW, b - KIHS. Experimental data: markers 1 - [47], 2 - [50].

In the region of the phase transition in silicon at an equilibrium melting temperature T_m, a positive enthalpy jump (Fig. 7) occurs, amounting to 9.1% and 9.5% for SW and KIHS potentials, respectively. In the case of superheating of the solid phase ΔT_{SW} = 715K and ΔT_{KIHS} = 565K, obtained with different potentials, the enthalpy continues to increase (Fig. 7). This energy is expended mainly on the thermal oscillations of the lattice. An increase in the

amplitude of the oscillations is associated with a decrease in the strength of the chemical bond of the crystal lattice and a transition to a lattice of a covalent-metallic and completely metallic type. With such structural changes in the lattice, the specific heat abruptly decreases. According to the MDM results, the jump value for the SW potential is 35%, and for the KIHS - 11%. The specific heat jump at the phase transition in accordance with the experimental data [50] is 6.4%. The difference in the specific heat at $T=T_m$ for SW and KIHS potentials in the solid phase is only ~ 3%, and in the liquid phase ~ 25%. Thus, a comparison of estimates of the jump in the specific heat at the phase transition from the calculated and experimental data [50, 47] shows that for the liquid phase, better results are obtained by using the KIHS potential. For a solid phase, a greater correspondence with experimental data is provided by the potential SW (Fig. 8).

	SW, a_k		**KIHS, a_k**	
k	**Solid, T_0 = 300K**	**Liqid, T_m = *1685K***	**Solid, T_0 = 300K**	**Liqid, T_m = *1685K***
0	2.066477761×10^{-4}	2.2144171×10^{-4}	2.696688598	$2.76559151883\times10^{-4}$
1	7.030246194×10^{-8}	-2.25388975×10^{-8}	4.564413181	$1.15115880659\times10^{-8}$
2	$-2.710486115\times10^{-12}$	$3.078427811\times10^{-11}$	-16.94440201	$1.03491212167\times10^{-11}$
3		6.83656818×10^{-14}		$-3.80421384573\times10^{-15}$
***Δ($P_m(T_i)$,y_i)* %**	*2.283*	*6.691*	*0.089*	*1.848*

Table 6. Values of the coefficients of functions approximating the specific heat of silicon based on the results of MDM and the magnitude of the approximation error.

The temperature dependences of the specific heat for SW and KIHS potentials were approximated by the following polynomials.

For solid phase: $C_{lat,sol}(T)=\left(a_0+a_1(T-T_0)+a_2(T-T_0)^2\right)_{SW,KIHS}$.

For liquid phase: $C_{lat,liq}(T)=\left(a_0+a_1(T-T_0)+a_2(T-T_0)^2+a_3(T-T_0)^3\right)_{SW,KIHS}$.

The values of the coefficients a_k and the approximation errors (5) are presented in Table 6.

4 CONCLUSIONS

In the paper, the equilibrium properties of crystalline and molten silicon have been obtained using molecular dynamics modeling (MDM) in the temperature range associated with the melting and crystallization of microstructures (300K ÷ 4000K). The pressure dependences of the latent heat of melting $L_m(P)$, and the equilibrium melting temperature $T_m(P)$, which is the equilibrium boundary between the two phases of silicon, solid and liquid, are determined. The temperature dependences of the density $\rho(T)$, the linear dimension of the sample $L(T)$, the linear expansion coefficient $\alpha(T)$, the enthalpy $H(T)$, and the specific heat of the lattice $C_{lat}(T)$ are also determined. MDM was performed with the potentials of Stillinger-Weber and KIHS. The simulation results showed that at the melting temperature $T=T_m$, at the melting-crystallization phase transition, the properties of silicon change abruptly. In the vicinity of the phase transition point, all the properties of crystalline silicon undergo qualitative changes and differ significantly from those of metals. The melting process leads to a substantial increase in the density $\rho(T)$, the linear expansion coefficient $\alpha(T)$, and the linear size $L(T)$. Such changes in properties are indicators of the condensation of silicon during

melting, in contrast to metals. As the temperature in the solid and liquid phases increases, the enthalpy $H(T)$ increases. At $T=T_m$, the enthalpy increases more than 9% by a jump. The heat capacity of the lattice $C_{lat}(T)$ in the solid phase increases with increasing temperature, at $T=T_m$, in a phase transition, in contrast to metals, abruptly decreases, after which it again increases in the liquid phase. Comparison of the calculated characteristics of silicon with experimental data has shown that for the solid phase the SW potential provides a greater correspondence with the experimental data, and for the liquid phase the KIHS potential is more acceptable. The properties of silicon in the melting range obtained with both potentials provide an acceptable qualitative and quantitative agreement with the experimental data. Numerical and graphical information on the obtained properties and results of comparison with experimental data are presented. The obtained dependences of the properties of silicon are approximated by polynomials of low degrees.

Acknowledgements: This study was supported by the Russian Science Foundation (project no. 18-11-00318) and the Competitiveness Enhancement Program of the MEPhI.

REFERENCES

[1] C. J. Glassbrenner and Glen A. Slack. “Thermal Conductivity of Silicon and Germanium from 3K to the Melting Point”, *Physical Review*, **134** (4a), A1058-A1069 (1964)

[2] S. Nakamura, T. Hibiya. Thermophysical properties data on molten semiconductors. International Journal of Thermophysics, **13** (6), 1061–1084 (1992)

[3] K. Sokolowski-Tinten and D. von der Linde, “Generation of dense electron–hole plasmas in silicon”, *Phys. Rev. B*, **61**, 2643–2650 (2000).

[4] Okada, T., and Ohno, S., “Electrical Properties of Liquid Si and Liquid Au–Si Alloys”, *J.Phys. Soc. Jpn.*, **72**, 352-356 (2003).

[5] Hidekazu Kobatake, Hiroyuki Fukuyama, Izuru Minato, Takao Tsukada, and Satoshi Awaji, “Noncontact measurement of thermal conductivity of liquid silicon in a static magnetic field”, *Appl. Phys. Let.,* **90**, 094102(1-3) (2007)

[6] Shaul Pearl, Nir Rotenberg, and Henry M. van Driel, “Three photon absorption in Silicon for 2300 – 3300 nm”, *App. Phys. Let.,* **93**, 131102(1-3) (2008)

[7] Magometov, Gadzhiev, “Vy`sokotemperaturnaia teploprovodnost` kremniia v tverdom i zhidkom sostoianiiakh”, *Teplofizika vy`sokikh temperatur*, **46** (3), 466-468 (2008)

[8] Inigo Liberal, Ahmed M. Mahmoud, Yue Li, Brian Edwards, Nader Engheta, “Photonic doping of epsilon-near-zero media”, *Science,* **355**, 1058–1062 (2017)

[9] D. Buta, M. Asta, and J. J. Hoyt, “Kinetic coefficient of steps at the Si(111) crystal-melt interface from molecular dynamics simulations,” *Journal of Chemical Physics*, **127**, no. 7, Article ID 074703(1-10) (2007).

[10] A. Mostafa, M. Medraj, “Review. Binary Phase Diagrams and Thermodynamic Properties of Silicon and Essential Doping Elements (Al, As, B, Bi, Ga, In, N, P, Sb and Tl)”, *Materials*, **10**, 676(1-49) (2017).

[11] A.E. Becquerel, “Mémoire Sur Les Effets Électriques Produits Sous L’influence Des Rayons Solaires”, *Ann. Phys. Chem.* **1841(***54)*, 35–42 (1839).

[12] Kozo Fujiwara, “Review Article. Crystal Growth Behaviors of Silicon during Melt Growth Processes”, *International Journal of Photoenergy*, **2012**, Article ID 169829(1-16) (2012).

[13] Jafar Safarian, Buhle Xakalashe and Merete Tangstad, "Vacuum removal of the impurities from different silicon melts", *26th European Photovoltaic Solar energy conference and exhibition*, 1810-1813 (2011).

[14] G. Coletti, *Impurities in Silicon and Their Impact on Solar Cell Performance*, Utrecht University: Utrecht, the Netherlands (2011).

[15] Wolfhard Möller and Subroto Mukherjee, "Plasma-based ion implantation", *Current Science*, **83** (3), 1-16 (2002)

[16] H.L. Sun, Woojin Lee, Knight Xu, H. Y. Tsun, K. T. Peng, L. S. Juang, and H. P. Tseng, "Backing up Medium Current Implanters using Single Wafer High Energy Implanter for Manufacturing Efficiency". *CP866, Ion Implantation Technology*, *ed. by K. J. Kirkby, R. Gwilliam, A. Smith, and D. Chivers, American Institute of Physics*, 385-388 (2006).

[17] J. Valenta, J. Linnros and R. Juhasz, J.-L. Rehspringer, F. Huber, and C. Hirlimann, S. Cheylan and R. G. Elliman, "Photonic band-gap effects on photoluminescence of silicon nanocrystals embedded in artificial opals", *JAP*, **93** (8), 4471-4474 (2003).

[18] Iu.N. Taran, V.Z. Kutcova, O.A. Nosko, "Fazovy`e perehody` poluprovodnik–metal", *Usp. Fiz. Met.*, **5**, 87–166 (2004).

[19] Urs Zywietz, Andrey B. Evlyukhin, Carsten Reinhardt & Boris N. Chichkov. "Laser printing of silicon nanoparticles with resonant optical electric and magnetic responses", *Nature Communications*, 1-7 (2014).

[20] V.I. Mazhukin, V.V. Nosov, U. Zemmler, "Issledovanie teplovy`kh i termouprugikh polei` v poluprovodnikakh pri impul`snoi` obrabotke", *Matematicheskoe modelirovanie,* **12**(2), 75-83 (2000).

[21] V.M. Glazov, V.B. Kol`tcov, V.Z. Kutcova i dr. "Strukturny`e prevrashcheniia pri nagreve monokristallov kremniia", *Fizika i tekhnika poluprovodnikov*, **25** (4), 558-595 (1991).

[22] V.I. Mazhukin, A.V. Shapranov, V.E. Perezhigin. "Matematicheskoe modelirovanie teplofizicheskikh svoi`stv, protcessov nagreva i plavleniia metallov metodom molekuliarnoi` dinamiki", *Mathematica Montisnigri*, **24**, 47 – 66 (2012).

[23] V.I. Mazhukin, A.V. Shapranov, A.E. Rudenko, "Sravnitel`ny`i` analiz potentcialov mezhatomnogo vzaimodei`stviia dlia kristallicheskogo kremniia", *Mathematica Montisnigri*, **30**, 56-75 (2014).

[24] M. Kaczmarski, O.N. Bedoya-Martı.nez, E.R. Hernandez, "Phase diagram of silicon from atomistic simulations", *Phys. Rev. Lett.*, **94,** 095701(1-4) (2005)

[25] V.P. Lipp, B. Rethfeld, M.E. Garcia, D.S. Ivanov, "Atomistic-continuum modeling of short laser pulse melting of Si targets", *Phys. Rev. B*, **90**, 245306(1-17) (2014).

[26] Mazhukin V.I., Shapranov A.V., Samokhin A.A., Ivochkin A.Yu., "Mathematical modeling of non-equilibrium phase transition in rapidly heated thin liquid film", *Mathematica Montisnigri*, **27**, 65 - 90 (2013).

[27] V.I. Mazhukin, A.A. Samokhin, A.V. Shapranov, M.M. Demin, P.A. Pivovarov, "Modeling and visualization of nanosecond laser vaporization of metals in near critical region", *Scientific Visualization*, **8** (1), 1-22 (2016).

[28] F. H. Stillinger and T. A. Weber, "Computer simulation of local order in condensed phases of silicon", *Phys. Rev. B*, **31**, 5262-5271 (1985).